HHS Public Access

Author manuscript

Biofabrication. Author manuscript; available in PMC 2020 December 11.

Published in final edited form as:

Biofabrication. ; 11(2): 025003. doi:10.1088/1758-5090/aafc49.

Bioprinting of 3D breast epithelial spheroids for human cancer models

Swathi Swaminathan, **Qudus Hamid**, **Wei Sun**, **Alisa Morss Clyne**

Department of Mechanical Engineering and Mechanics, Drexel University, Philadelphia, PA 19104, United States of America

Abstract

3D human cancer models provide a better platform for drug efficacy studies than conventional 2D culture, since they recapitulate important aspects of the *in vivo* microenvironment. While biofabrication has advanced model creation, bioprinting generally involves extruding individual cells in a bioink and then waiting for these cells to self-assemble into a hierarchical 3D tissue. This self-assembly is time consuming and requires complex cellular interactions with other cell types, extracellular matrix components, and growth factors. We therefore investigated if we could directly bioprint pre-formed 3D spheroids in alginate-based bioinks to create a model tissue that could be used almost immediately. Human breast epithelial cell lines were bioprinted as individual cells or as pre-formed spheroids, either in monoculture or co-culture with vascular endothelial cells. While individual breast cells only spontaneously formed spheroids in Matrigel-based bioink, pre-formed breast spheroids maintained their viability, architecture, and function after bioprinting. Bioprinted breast spheroids were more resistant to paclitaxel than individually printed breast cells; however, this effect was abrogated by endothelial cell co-culture. This study shows that 3D cellular structure bioprinting has potential to create tissue models that quickly replicate the tumor microenvironment.

Keywords

3D bioprinting; breast cancer; endothelial cells; 3D cancer model; bioink; paclitaxel; co-culture

1. Introduction

Physiologically relevant 3D human cancer models are needed as intermediaries between conventional 2D cell culture and human disease [1, 2]. For breast cancer in particular, healthy and cancerous breast epithelial cells cultured in 3D basement membrane-like matrices self-organize into spherical, polarized structures or complex ductal networks that resemble the *in vivo* tissue architecture [3–7]. 3D cancer models can incorporate many additional aspects of the cancer microenvironment, including heterogeneous cell types, varied extracellular matrix composition and mechanical properties, as well as growth factor and cytokine gradients [8, 9]. Since each of these factors, individually and in combination, has been shown to impact healthy and cancerous breast epithelial cell structure and function,

asm67@drexel.edu.

it is essential that drug testing occur in 3D cancer models that better recapitulate the physiological *in vivo* microenvironment [10].

Biofabrication shows great promise in creating 3D cancer models [11–13]. Bioprinting, in which living cells and extracellular matrix 'bioink' are printed together, allows tight spatial control over initial cell and growth factor location, which can promote formation of the appropriate tissue architecture [14]. A variety of natural and synthetic hydrogels, including Matrigel, fibrin, collagen, polyethylene glycol, alginate, and gelatin-methacrylate can be bioprinted and have been used to study cancer cell function and invasion [15–18]. We recently 3D printed Hela cells in a gelatin/alginate/fibrinogen hydrogel to create an *in vitro* cervical cancer model. The bioprinted 3D tumor cells showed a higher proliferation rate, greater tendency to form spheroids, increased matrix metalloproteinase expression, and higher chemoresistance than cells in 2D culture [19]. These outcomes were more similar to *in vivo* responses, which suggests that bioprinted 3D human cancer models may better predict drug efficacy than conventional 2D cell culture or animal models.

Cancer interactions with the vasculature are of particular interest. Two of the most important factors in cancer mortality, angiogenesis (the growth of new blood vessels from existing vessels) and metastasis (cancer cell escape from the primary tumor into the bloodstream), rely on interactions between cancer and vasculature. Many different 3D tissue models have been created to study how vascular endothelial cells interact with cancer cells, including co-culture of tumor cells with endothelial cells or explanted vessels [20–22]. In some cases, endothelial cells are seeded within hollow channels to form a larger blood vessel and surrounded by a tumor cell-laden hydrogel, which then stimulates the endothelial cells to form a vascular network [23, 24]. We recently induced endothelial cells to form vascular tubes on Matrigel and then seeded pre-formed breast epithelial spheroids onto the vascular tubes [25]. While this model enabled the study of 3D endothelial-cancer interactions, it lacked consistency in spheroid location and Matrigel properties and was inherently low throughput due to the manual fabrication technique.

3D human cancer model biomanufacturing would enable advanced study of healthy and diseased cells and provide a powerful platform for drug screening [26, 27]. However, high throughput production of these models is limited by current biofabrication techniques. Currently, bioink composed of cells encapsulated within a matrix material is printed layer-by-layer in a specific pattern which guides the cells towards self-organization into the desired 3D architecture that hopefully recapitulates the *in vivo* tissue. Unfortunately, cellular self-assembly may take days or weeks, may require complex spatial and temporal environmental cues, or may not occur when two cell types (e.g. cancer cells, endothelial cells) are cultured together [11, 19, 28]. Therefore, different approaches are needed in 3D tissue biomanufacturing.

The objective of this study was to determine if we could bioprint multicellular building blocks, in this case breast epithelial spheroids, in different bioinks directly into a structure that could be used to test a functional response almost immediately. We now demonstrate that bioprinted breast spheroids remain viable and maintain their architecture and polarity in several bio-printing-friendly alginate-based bioinks. The breast spheroids can be bioprinted

into a co-culture grid structure to study endothelial interactions. Finally, we show that both 2D versus 3D breast epithelial cell architecture, as well as endothelial co-culture, alter cell viability in response to chemotherapy drugs. This method could decrease the time between bioprinting and assay from weeks to days; increase physiological relevance of *in vitro* cancer models by improving tissue architecture; and enable the use of primary human tissues with their stromal cells and matrix.

2. Materials and methods

2.1. Cell culture

Breast epithelial cell lines MCF10A, MCF10A-NeuN, MDA-MB-231 and MCF7 were a generous gift from Dr Mauricio Reginato (Drexel College of Medicine). MCF10A cells are a non-tumorigenic breast epithelial cell line derived from a patient with fibrocystic disease [29]. These cells are immortalized and do not express estrogen receptor. MCF10A cells polarize and organize into acinus-like spheroids with a hollow lumen when cultured on Matrigel. This 3D MCF10A spheroid does not represent normal breast tissue but is useful for dissecting cell-cell interactions in mammary glands. MCF10A-NeuN are MCF10A cells transfected to overexpress epidermal growth factor receptor 2 (Neu/HER2/ErbB2), which is commonly overexpressed in breast cancer and yields a poor prognosis [30]. These cells were used to study the specific effect of Neu/HER2/ErbB2 overexpression in bioprinting and the co-culture model. The MDA-MB-231 cell line is a triple-negative human breast cancer epithelial cell line lacking estrogen receptor, progesterone receptor, and epidermal growth factor receptor 2 [31]. MDA-MB-231 was established from the pleural effusion of a female patient with metastatic mammary adenocarcinoma and represents an aggressive, invasive and poorly differentiated breast cancer. The MCF7 cell line was also derived from the pleural effusion of a female patient with metastatic malignant adenocarcinoma; however, MCF7 cells have estrogen and progesterone receptors and are tumorigenic only with hormone supplementation [32]. These cell lines were selected for this study since they represent a spectrum of breast epithelial biology and are used in the majority of breast cancer studies.

MCF10A and MCF10A-NeuN cells were cultured in DMEM/F12 (Corning, Manassas,VA) supplemented with 5% horse serum (Invitrogen, Waltham, MA), 20 ng ml^{-1} epidermal growth factor (EGF; Peprotech, Rocky Hill, NJ), 10 μg ml^{-1} bovine insulin (Sigma, St. Louis, MO), 10 ng ml^{-1} cholera toxin (Enzo Life Sciences, Farmingdale, NY), 500 ng ml^{-1} hydrocortisone (Sigma), and 1% penicillin-streptomycin (Invitrogen). MDA-MB-231 cells were cultured in DMEM (Corning) supplemented with 10% fetal bovine serum (FBS; Hyclone, Logan, UT) and 1% penicillin-streptomycin. MCF-7 cells were cultured in the same medium as MDA-MB-231 cells with 10 μg ml^{-1} bovine insulin (Sigma). Human umbilical vein endothelial cells (HUVEC, Cell Applications, San Diego, CA) were cultured in endothelial growth medium-2 (EGM-2; Lonza, Allendale, NJ) supplemented with 10% FBS and 1% penicillin-streptomycin All cells were maintained in a humidified environment at 37 °C and 5% CO_2, with a medium change every two days. Breast epithelial cell lines were used up to passage 25, and HUVEC were used up to passage 9.

2.2. 3D breast spheroid formation

To grow 3D breast spheroids, 30 μl growth factor reduced Matrigel (Corning) was added to each well of a Falcon 8 chamber polystyrene vessel affixed to a tissue culture treated glass slide (Corning) and incubated at 37 °C for 20 min to solidify the Matrigel. Breast epithelial cells were trypsinized and resuspended in their respective growth medium with 20% Matrigel, and 5000 cells were added to each chamber well. MCF10A cells formed spheroids in 8–10 d, whereas MCF-7, MDA-MB-231 and MCF10A-NeuN cells formed spheroids within 5–6 d. Medium was replaced every 4 d.

2.3. Mono- and co-culture biofabrication

A dual nozzle bio-deposition system based on a rapid prototyping platform was used for biofabrication. The system consists of three motion arms that allow micron-scale spatial control of material deposition as well as two screw driven motors that can deposit biological material from 10 ml syringes. This 3D printing system was functionalized with a high-efficiency particulate air filtration system as well as UV-sterilization capabilities to maintain a sterile environment during bioprinting. An independent syringe heating enclosure (SunP Biotech LLC, Cherry Hill, NJ) was also used to control bioink temperature in the syringe.

Cells and spheroids were printed in three different bioinks: Matrigel, gelatin-alginate, and collagen-alginate. Matrigel is the standard biomaterial used to create 3D breast epithelial spheroids. However, Matrigel is difficult to work with since it gels at temperatures above 4 °C, necessitating working quickly and keeping all components that touch the Matrigel at low temperature. Matrigel is also expensive and has significant batch-to-batch variability, since it is derived from Engelbreth-Holm-Swarm mouse sarcoma cells. We therefore determined if less expensive and temperature insensitive bioinks like alginate could be used to bioprint 3D breast epithelial spheroids. The Matrigel bioink consisted of medium with 2% (v/v) Matrigel. The gelatin-alginate bioink consisted of medium mixed with 10% (w/v) gelatin (Sigma) and 1% (w/v) sodium alginate (Sigma) in 0.9% sodium chloride (NaCl; Fisher Scientific). The collagen-alginate bioink consisted of medium mixed with 3% alginate and 0.025% collagen in 0.9% NaCl.

Breast epithelial cells or vascular endothelial cells were mixed at 2×10^6 cells ml^{-1} in each bioink. Spheroid concentration was not quantified, since the spheroid size (~100 μm) was too large for our cell counter. Instead, spheroids were counted in low magnification phase contrast microscopy images after bio-printing. Bioprinted spheroid density was 120–150 spheroids cm^{-2}. The cell-laden bioink was drawn into a 10 ml syringe and capped with a 25 gauge nozzle tip. The syringe was encased in a 37 °C heating element to prevent the bioink from gelling. For gelatin-alginate or collagen-alginate bioink, the bioink syringe was placed in a coaxial needle and connected to a second 10 ml syringe with 3% (w/v) calcium chloride ($CaCl_2$; VWR, Radnor, PA) to enable rapid gelling of the alginate.

For preliminary experiments, 60–120 μl cell-laden bioink was microextruded at 1 ml min^{-1}. After alginate-based structures were printed, 3% $CaCl_2$ was added for 3 min to chemically crosslink the construct. Medium was then added to each well to cover the construct. Constructs were incubated at 37 °C and 5% CO_2 for 24–96 h, after which they were labelled

and imaged by confocal microscopy. To create the interconnected co-culture system, a 10 × 10 × 1 mm grid was fabricated from epithelial and endothelial cell-laden bioinks. Six intersecting layers were printed at vertical increments of 0.015 cm by forced extrusion at 3 mm s^{-1} in a sterile atmosphere at 37 °C. For co-cultures, three breast epithelial cell layers were printed followed by three endothelial cell layers. The constructs were then immersed in 3% $CaCl_2$ for 3 min to completely crosslink the alginate. Each mono- or co-culture construct was then transferred to a 35 mm tissue culture dish in the appropriate growth medium containing 10 ng ml^{-1} EGF and 2% Matrigel.

2.4. Confocal microscopy

To prepare samples for confocal microscopy, mono- and co-cultures were fixed with 4% paraformaldehyde for one hour at room temperature. Samples were then blocked with immunofluorescence (IF) buffer (130 mM NaCl, 7 mM Na_2HPO_4, 3.5 mM NaH_2PO_4, 7.7 mM NaN_3, 0.1% bovine serum albumin (BSA; Sigma), 0.2% Triton X-100, and 0.05% Tween-20, pH 7.4) with 10% goat serum for 90 min (primary block), followed by 40 min with IF buffer plus 10% goat serum and Affinipure $F(ab')_2$ fragment goat anti-mouse IgG (115-006-020, 1:100; Jackson ImmunoResearch, West Grove, PA; secondary block). MCF10A and MCF10A-NeuN cell lines express integrin $\alpha 6$, which is important for showing spheroid polarization and morphology. Therefore samples from these two cell lines were then incubated with a primary antibody for integrin $\alpha 6$ (MAB1378, 1:100, Millipore, Billerica, MA) in secondary blocking buffer overnight at 4 °C, followed by an Alexa Fluor 488 secondary antibody (A-11006, 1:200; Invitrogen) and Hoescht 33342 (62249, 1:1000, Thermo Scientific, Waltham, MA) for one hour at room temperature protected from light. MDA-MB-231 and MCF7 cell lines do not express high levels of integrin $\alpha 6$, and therefore these cell lines were incubated with rhodamine phalloidin (A12379, 1:200, Thermo Scientific, Waltham, MA) to visualize actin filaments with Hoescht 33342 overnight at 4 °C protected from light. After thorough washing, samples were mounted on coverslips in PBS-Glycine. Samples were then imaged using either an LSM 700 (Zeiss, Thornwood, NY) or FV1000 (Olympus, Waltham, MA) confocal microscope. The images were obtained as z stacks of ~25 slices in 5 μm steps, and all z planes were compressed into a single plane using the Extended Focus command in Volocity 6.3 cell imaging software (Perkin Elmer, Hopkinton, MA).

2.5. Functional assays of bioprinted structures

Cell viability was assessed in bioprinted structures using a Live/Dead assay (Invitrogen) and resazurin (Sigma, St.Louis, MO) as per manufacturer's instructions. For the Live/Dead assay, 0.5 μM calcein-AM (live cells) and 1 μM ethidium bromide (dead cells) were added to samples in PBS. After a 20 min incubation at room temperature, samples were imaged by confocal microscopy. For viability assessment in co-cultures, HUVECs and breast epithelial cells were distinguished in ImageJ via size and positional analysis using the particle analyzer plugin. Cell viability was further assessed using resazurin. Conditioned medium from bioprinted structures was transferred to a 96-well plate and incubated with 5% v/v resazurin (0.1 mg ml^{-1}) in phenol red-free DMEM medium for two hours at 37 °C. Absorbance was measured in a microplate reader (Synergy H1, Biotek, VT) and data were collected at 570 nm using the Gen5 software.

2.6. Statistical analysis

Statistical analyses were conducted in GraphPad Prism software. All data are shown as mean +/− standard deviation. Two groups were compared using Student's t-test, and multiple groups were compared by ANOVA with Tukey-Kramer post-hoc test. All experiments were conducted at least three times with three samples per experiment.

3. Results and discussion

3.1. Bioprinting individual breast cells

3D *in vitro* culture of breast epithelial cells better replicates many aspects of *in vivo* tissue function; however, protocols for forming 3D breast spheroids generally required Matrigel, which is expensive, has significant batch-to-batch variability, and is difficult to bioprint due to its temperature sensitivity. We therefore tested whether individual breast epithelial cells would form 3D spheroids when bioprinted in bioinks that are lower cost, more consistent, and temperature insensitive. When individual MCF10A (non-tumorigenic) and MCF10A-NeuN, MDA-MB-231, and MCF-7 (cancerous) breast cells were extrusion printed in Matrigel, gelatin-alginate, or collagen-alginate-based bioinks, 81%–96% of cells were viable after 24 h (Live/Dead assay; representative images in figure 1(A) with quantification in figure 1(B)). The only bioprinted combinations that demonstrated cell viability lower than 90% were MCF10A-NeuN cells (82.4%) and MCF7 cells (81%) in collagen-alginate bioink, perhaps indicating that cells with high levels of growth factor and hormone receptors are less viable in collagen-alginate. Overall, these data demonstrate that both non-tumorigenic and cancerous breast epithelial cells could effectively be printed in a variety of bioinks. However, after five to eight days of culture, 3D breast epithelial spheroids only formed in Matrigel and not the alginate-based bioinks (figure 1(C); inset shows polarized hollow MCF10A spheroid). Breast epithelial cells printed in either gelatin-alginate or collagen-alginate bioinks formed a 2D monolayer. These data suggest that the prominent Matrigel protein laminin is a critical factor in breast epithelial spheroid formation, as described in previous studies [4]. Thus if 3D breast spheroids are to be incorporated into bioprinted structures formed of non-Matrigel bioinks, alternative bioprinting techniques are needed.

3.2. Bioprinting 3D breast spheroids

Since individual breast epithelial cells did not spontaneously form 3D spheroids when bioprinted in non-Matrigel bioinks, we bioprinted pre-formed spheroids in alginate-based bioinks and measured cell viability and spheroid morphology. When pre-formed 3D breast spheroids were bioprinted in Matrigel, gelatin-alginate, and collagen-alginate-based bioinks, 82%–98% of breast epithelial cells were again viable in all of the bioinks after 24 h (representative confocal microscopy images in figure 2(A), quantification in figure 2(B)). After 48 h, breast spheroids maintained the typical morphology that was observed prior to bioprinting for the given cell type, irrespective of the bioink (figure 2(C); insets show polarized hollow MCF10A spheroids). Non-tumorigenic MCF10A breast epithelial spheroids displayed a hollow center, with integrin $\alpha 6$ polarized to the outside edge of the spheroid. Cancerous MCF10A-NeuN breast epithelial cell formed polarized spheroids without hollow centers, while cancerous MDA-MB-231 and MCF-7 breast epithelial cells formed irregular spheroids. We further evaluated bioprinted spheroid viability and

morphology over 96 h post-printing (figure 3; insets show polarized hollow MCF10A spheroids) as well as an additional 72 h (data not shown), for a total culture time of seven days. All spheroids had intact cell membranes and nuclei, indicating that viability was maintained in long-term culture. MCF10A and MCF10A-NeuN spheroids maintained their pre-printing morphology for the entire time; however, spheroids that were in close proximity began to join together to form megaspheroids. MDA-MB-231 and MCF-7 spheroids maintained their pre-printing morphology for 72 h and then started to proliferate and migrate out of the spheroids over the next 24–96 h. This invasive behavior is also observed in these spheroids when they are maintained in the original Matrigel culture without bioprinting.

These data demonstrate that pre-formed 3D breast epithelial spheroids can be bioprinted in various bioinks without loss of viability or morphology. Several techniques could be added to this method to further control spheroid size and concentration. Spheroid size could be controlled in self-assembled spheroids by using cell strainers, which can be sequentially employed to ensure that printed spheroids fall within a specific size range. Alternatively, the spheroids themselves could be biofabricated. Shi *et al* recently created controlled size spheroids by sparsely seeded cells and then culturing them into cell islands. The cell islands were then detached and shaken in media with dispase, which caused the cell sheets to curl and form spheroids. Spheroid size was controlled by the initial cell sheet culture time [33]. Spheroid concentration could be controlled either by counting spheroids after formation or by controlling the initial cell seeding density in the method by Shi *et al* While the optimal spheroid concentration in the 3D structure is likely dependent on the application, in this study we maximized spheroid density while maintaining at least 100 μm between spheroids. When spheroids are too close, they join together to form megaspheroids with the associated loss of spheroid morphology.

3.3. Breast epithelial cell co-culture with endothelial cells

Our long-term goal is to bioprint 3D breast epithelial spheroids within an endothelialized microvascular network to determine interactions between these two cell types in a physiologically relevant structure. We first tested whether individual breast epithelial cells and vascular endothelial cells would remain viable in 3D bioprinted culture, since endothelial cells died in our previous experience with 2D breast epithelial co-culture [34]. We therefore bioprinted HUVEC with either non-tumorigenic MCF10A or cancerous MDA-MB-231 individual breast epithelial cells in a six layer collagen-alginate grid structure (figure 4(A)). These structures were already proven to have good mechanical properties and sustain layer-by-layer fabrication [35]. 24 h after bioprinting, 92%–99% of MCF10A and HUVEC and 85%–89% of MDA-MB-231 and HUVEC remained viable in both mono and co-cultures (figure 4(B)). We next determined if 3D breast epithelial spheroids and vascular endothelial cells would remain viable in the collagen-alginate grid structure. Again, we showed high cell viability for 3D breast spheroids and HUVECs in both mono and co-culture, with the only viability lower than 90% being for HUVEC in the MDA-MB-231 experiments (figure 5).

3.4. Drug response in 2D and 3D bioprinted breast epithelial—vascular endothelial cell co-culture

Finally, we quantified cell viability (via resazurin and Live/Dead assay) within the bioprinted structures in response to paclitaxel, a chemotherapeutic agent used to treat many types of cancer including breast cancer. Endothelial cells bioprinted in collagen-alginate bioink showed decreasing viability with increasing paclitaxel concentration, as expected. Both MCF10A and MDA-MB-231 breast epithelial cells showed decreasing viability with increasing paclitaxel dose. However, breast epithelial cells printed as 3D spheroids showed higher viability at all paclitaxel doses, suggesting that 3D spheroids are more resistant to paclitaxel than individual cells. Interestingly, the paclitaxel resistance seen in 3D breast spheroids was abrogated when breast epithelial cells were bioprinted together with endothelial cells (figure 6(A)). Upon closer examination of HUVEC, MCF10A, and MDA-MB-231 viability via the Live/Dead assay (figure 6(B)), it was clear that the majority of cell death, in particular at lower paclitaxel concentrations, occurred in the endothelial cells. At the highest paclitaxel concentration (200 nM), the majority of HUVEC were dead. While most of the MCF10A and MDA-MB-231 spheroids remained viable, they lost their morphology and began to disperse within the bioprinted structure. Therefore it is possible that the decrease in resazurin fluorescence at higher paclitaxel concentrations in HUVEC-breast epithelial spheroid co-culture relates to loss of breast cell metabolic activity, rather than cell death.

These data now show for the first time that 3D cellular structures can be bioprinted while maintaining not only cell viability but also 3D architecture, polarization, and function. While clusters of homo- or heterogeneous cell types are often called spheroids, these spheroids are a cell amalgamation without a specific architecture or polarization. Bioprinting has in fact been used to improve both the speed and reproducibility of this type of spheroid production [36, 37]. The breast epithelial spheroids used in our study, in particular those derived from non-tumorigenic cells, show integrin $\alpha 6$ polarization to the outer spheroid edge and a hollow center both before and after printing, showing that the physical stress induced by the printing process did not significantly change their architecture or polarization. We also showed that the bioprinted spheroids remain more resistant to chemotherapeutic agents, as has been shown by other groups, indicating that they also retain function [38, 39]. Thus it is possible that other complex 3D multicellular structures, including microvessels derived from adipose tissue or patient derived tumor samples, could be bioprinted to explore angiogenesis or to create an *in vitro* patient derived xenograft (PDX) model.

In our study, we bioprinted the spheroids in alginate-based bioinks, which are largely inert other than the natural matrix proteins that we included. However, spheroids could likely be printed in a wide variety of bioinks, both natural and synthetic, that better replicate the *in vivo* tumor microenvironment. Many studies in recent years have shown that both extracellular matrix and stromal cells are critical to determining cancerous cell responses. The specific proteins present and their fiber alignment, together with matrix stiffness, density, and porosity, have been shown to impact angiogenesis, cancer cell migration and metastasis, and matrix metalloproteinase expression [10–12]. In addition, stromal cells such as fibroblasts and immune cells affect cancer cells directly via cytokine and inflammatory

factor release or indirectly via extracellular matrix alterations [40, 41]. In the future, breast cancer associated extracellular matrix proteins could be incorporated into the bioink along with stromal cells to provide essential biochemical and adhesive cues to the cancer spheroids.

We also found that using alginate as the bioink came with unintended consequences. We had initially proposed to measure glucose metabolism in bioprinted breast epithelial and vascular endothelial cell co-cultures via $^{13}C_6$-glucose mass spectrometry. When we collected conditioned media and extracted cell lysates from the bioprinted alginate structures, the mass spectrometry results showed that labelled lactate and pyruvate were higher in bioprinted structures that included MDA-MB-231 cancerous cells in comparison to structures with MCF10A or endothelial cells. This is in keeping with published reports that cancer cells metabolize more glucose than normal cells [42]. However, total unlabeled pyruvate in all lysates from collagen-alginate bioprinted structures was extremely high. Upon further study, we discovered evidence that alginate can be degraded into pyruvate [43, 44]. Thus alginate-based bioinks may not be suitable for *in vitro* metabolism studies as the alginate degradation products may alter the metabolic fuels available to cells.

A primary question remains for why co-cultures of vascular endothelial cells and breast epithelial cells abrogated the increased chemoresistance of 3D culture. Paclitaxel has been shown to have anti-angiogenic properties [45]. In our own work and in the literature, paclitaxel induces endothelial cell death at much lower doses than are required for breast epithelial cells. Paclitaxel downregulates important angiogenic factors like vascular endothelial growth factor (VEGF) and angiopoetin-1 (Ang-1), while increasing thrombospondin-1 (TSP-1) secretion by endothelial cells [46, 47]. TSP-1 at high doses has been shown to decrease breast cancer proliferation [48]. TSP-1 also may decrease breast epithelial cell-cell adhesion and increase invasion, which could cause spheroids to lose their 3D architecture and thereby have similar paclitaxel sensitivity as individual cells [49].

For spheroid bioprinting to become a practical reality, spheroid production needs to be accelerated and optimized. One possibility would be to use microdroplet printing to create highly parallel spheroid production, although this technique is still limited in its throughput and reproducibility. Another option is to directly engineer the spheroids, with the polarized structure and hollow center, through other biofabrication means (e.g. detaching cell sheets and stimulating them to form spheroids) [33]. Alternatively, this technique could move directly to tumor-derived tissues, which have significant advantages over cell line based spheroids, in which throughput would be limited only by the tumor size.

4. Conclusion

This research shows for the first time the possibility of bioprinting multicellular breast tumor spheroids while maintaining spheroid structure, polarization, and function. These spheroids can be bioprinted into co-culture systems, which can then be used almost immediately for assays such as drug screening. We believe that 3D multicellular structure bioprinting has great potential to rapidly create tissue models that better replicate the structure and function of the *in vivo* tumor microenvironment. In the future, we plan to bioprint 3D breast cancer

spheroids with 3D microvessels in varied bioinks to measure metabolic interactions between these two cell types.

References

[1]. Garcia J, Yang Z, Mongrain R, Leask RL and Lachapelle K 2018 3D printing materials and their use in medical education: a review of current technology and trends for the future BMJ Simul.Technol. Enhanc. Learn 4 27–40

[2]. Jang J, Yi H-G and Cho D-W 2016 3D printed tissue models: present and future ACS Biomater. Sci. Eng 2 1722–31

[3]. Barcellos-Hoff MH, Aggeler J, Ram TG and Bissell MJ 1989 Functional differentiation and alveolar morphogenesis of primary mammary cultures on reconstituted basement membrane Development 105 223–35 [PubMed: 2806122]

[4]. Debnath J, Muthuswamy SK and Brugge JS 2003 Morphogenesis and oncogenesis of MCF-10A mammary epithelial acini grown in three-dimensional basement membrane cultures Methods 30 256–68 [PubMed: 12798140]

[5]. Petersen OW, Ronnov-Jessen L, Howlett AR and Bissell MJ 1992 Interaction with basement membrane serves to rapidly distinguish growth and differentiation pattern of normal and malignant human breast epithelial cells Proc. Natl Acad. Sci. USA 89 9064–8

[6]. Weaver VM et al. 1997 Reversion of the malignant phenotype of human breast cells in three-dimensional culture and *in vivo* by integrin blocking antibodies J. Cell Biol 137 231–45 [PubMed: 9105051]

[7]. Sokol ES, Miller DH, Breggia A, Spencer KC, Arendt LM and Gupta PB 2016 Growth of human breast tissues from patient cells in 3D hydrogel scaffolds Breast Cancer Res. 18 19 [PubMed: 26926363]

[8]. Radisky D, Muschler J and Bissell MJ 2002 Order and disorder: the role of extracellular matrix in epithelial cancer Cancer Invest. 20 139–53 [PubMed: 11852996]

[9]. Schmeichel KL and Bissell MJ 2003 Modeling tissue-specific signaling and organ function in three dimensions J Cell Sci. 116 2377–88 [PubMed: 12766184]

[10]. Asghar W, El Assal R, Shafiee H, Pitteri S, Paulmurugan R and Demirci U 2015 Engineering cancer microenvironments for *in vitro* 3D tumor models Mater Today 18 539–53

[11]. Zhang YS, Duchamp M, Oklu R, Ellisen LW, Langer R and Khademhosseini A 2016 Bioprinting the cancer microenvironment ACS Biomater. Sci. Eng 2 1710–21

[12]. Belgodere JA, King CT, Bursavich JB, Burow ME, Martin EC and Jung JP 2018 Engineering breast cancer microenvironments and 3D bioprinting Front Bioeng. Biotechnol. 6 66

[13]. Wang C, Tang Z, Zhao Y, Yao R, Li L and Sun W 2014 Three-dimensional *in vitro* cancer models: a short review Biofabrication 6 022001 [PubMed: 24727833]

[14]. Zhang YS, Duchamp M, Oklu R, Ellisen LW, Langer R and Khademhosseini A 2016 Bioprinting the cancer microenvironment ACS Biomater. Sci. Eng 2 1710–21

[15]. Liu J et al. 2012 Soft fibrin gels promote selection and growth of tumorigenic cells Nat. Mater. 11 734–41

[16]. Pedron S and Harley BA 2013 Impact of the biophysical features of a 3D gelatin microenvironment on glioblastoma malignancy J. Biomed. Mater. Res. A 101 3404–15 [PubMed: 23559545]

[17]. Raeber GP, Lutolf MP and Hubbell JA 2005 Molecularly engineered PEG hydrogels: a novel model system for proteolytically mediated cell migration Biophys. J 89 1374–88 [PubMed: 15923238]

[18]. Kaemmerer E, Melchels FP, Holzapfel BM, Meckel T, Hutmacher DW and Loessner D 2014 Gelatine methacrylamide-based hydrogels: an alternative three-dimensional cancer cell culture system Acta Biomater. 10 2551–62 [PubMed: 24590158]

[19]. Zhao Y. et al. 2014; Three-dimensional printing of Hela cells for cervical tumor model *in vitro*. Biofabrication. 6:035001. [PubMed: 24722236]

[20]. Seano G et al. 2013 Modeling human tumor angiogenesis in a three-dimensional culture system Blood. 121 e129–37 [PubMed: 23471306]

[21]. Verbridge SS, Chandler EM and Fischbach C 2010 Tissue-engineered three-dimensional tumor models to study tumor angiogenesis Tissue Eng. A 16 2147–52

[22]. Phamduy TB, Sweat RS, Azimi MS, Burow ME, Murfee WL and Chrisey DB 2015 Printing cancer cells into intact microvascular networks: a model for investigating cancer cell dynamics during angiogenesis Integr Biol. 7 1068–78

[23]. Chrobak KM, Potter DR and Tien J 2006 Formation of perfused, functional microvascular tubes *in vitro* Microvasc Res. 71 185–96 [PubMed: 16600313]

[24]. Ghajar CM et al. 2013 The perivascular niche regulates breast tumour dormancy Nat. Cell Biol. 15 807–17

[25]. Swaminathan S, Ngo O, Basehore S and Clyne AM 2017 Vascular endothelial-breast epithelial cell coculture model created from 3D cell structures ACS Biomater. Sci. Eng 3 2999–3006

[26]. Charbe N, McCarron PA and Tambuwala MM 2017 Three-dimensional bio-printing: a new frontier in oncology research World J. Clin. Oncol 8 21–36

[27]. Jackson SJ and Thomas GJ 2017 Human tissue models in cancer research: looking beyond the mouse Dis Model Mech. 10 939–42 [PubMed: 28768734]

[28]. Ouyang L, Yao R, Mao S, Chen X, Na J and Sun W 2015 Three-dimensional bioprinting of embryonic stem cells directs highly uniform embryoid body formation Biofabrication 7 044101 [PubMed: 26531008]

[29]. Qu Y. et al. 2015; Evaluation of MCF10A as a reliable model for normal human mammary epithelial cells. PLoS One. 10:e0131285. [PubMed: 26147507]

[30]. Haenssen KK et al. 2010 ErbB2 requires integrin alpha5 for anoikis resistance via Src regulation of receptor activity in human mammary epithelial cells J. Cell Sci 123 1373–82 [PubMed: 20332114]

[31]. Chavez KJ, Garimella SV and Lipkowitz S 2010 Triple negative breast cancer cell lines: one tool in the search for better treatment of triple negative breast cancer Breast Dis. 32 35–48 [PubMed: 21778573]

[32]. Levenson AS and Jordan VC 1997 MCF-7: the first hormone-responsive breast cancer cell line Cancer Res. 57 3071–8 [PubMed: 9242427]

[33]. Shi W. et al. 2018; Faciletumor spheroids formation in large quantity with controllable size and highuniformity. Sci. Rep. 8:6837. [PubMed: 29717201]

[34]. Swaminathan S, Ngo O, Basehore S and Clyne AM 2017 Vascular endothelial-breast epithelial cell coculture model created from 3D cell structures ACS Biomater. Sci. Eng 3 2999–3006

[35]. Wu Z, Su X, Xu Y, Kong B, Sun W and Mi S 2016 Bioprinting three-dimensional cell-laden tissue constructs with controllable degradation Sci. Rep 6 24474 [PubMed: 27091175]

[36]. Ling K, Huang G, Liu J, Zhang X, Ma Y, Lu T and Feng X 2015 Bioprinting-based high-throughput fabrication of three-dimensional MCF-7 human breast cancer cellular spheroids Engineering 1 269–74

[37]. Hribar KC et al. 2015 Nonlinear 3D projection printing of concavehydrogel microstructures for long-term multicellular spheroid and embryoid body culture Lab Chip 15 2412–8 [PubMed: 25900329]

[38]. Imamura Y et al. 2015 Comparison of 2D- and 3D-culture models as drug-testing platforms in breast cancer Oncol Rep. 33 1837–43 [PubMed: 25634491]

[39]. Zhu W, Holmes B, Glazer RI and Zhang LG 2016 3D printed nanocomposite matrix for the study of breast cancer bone metastasis Nanomedicine 12 69–79 [PubMed: 26472048]

[40]. Fullar A. et al. 2015; Remodeling of extracellular matrix by normal and tumor-associated fibroblasts promotes cervical cancer progression. BMC Cancer. 15:256. [PubMed: 25885552]

[41]. Gajewski TF, Schreiber H and Fu YX 2013 Innate and adaptive immune cells in the tumor microenvironment Nat. Immunol 14 1014–22 [PubMed: 24048123]

[42]. Yang DQ, Freund DM, Harris BR, Wang D, Cleary MP and Hegeman AD 2016 Measuring relative utilization of aerobic glycolysis in breast cancer cells by positional isotopic discrimination FEBS Lett. 590 3179–87 [PubMed: 27531463]

[43]. Kawai S et al. 2014 Bacterial pyruvate production from alginate, a promising carbon source from marine brown macroalgae J. Biosci. Bioeng 117 269–74 [PubMed: 24064299]

[44]. Doi H et al. 2017 Identification of enzymes responsible for extracellular alginate depolymerization and alginate metabolism in Vibrio algivorus Appl. Microbiol. Biotechnol 101 1581–92

[45]. Bocci G, Di Paolo A and Danesi R 2013 The pharmacological bases of the antiangiogenic activity of paclitaxel Angiogenesis. 16 481–92 [PubMed: 23389639]

[46]. Bocci G, Francia G, Man S, Lawler J and Kerbel RS 2003 Thrombospondin 1, a mediator of the antiangiogenic effects of low-dose metronomic chemotherapy Proc. Natl Acad. Sci. USA 100 12917–22 [PubMed: 14561896]

[47]. Hata K et al. 2004 Evaluation of the antiangiogenic effect of Taxol in a human epithelial ovarian carcinoma cell line Cancer Chemother Pharmacol. 53 68–74

[48]. Hyder SM, Liang Y and Wu J 2009 Estrogen regulation of thrombospondin-1 in human breast cancer cells Int. J. Cancer 125 1045–53 [PubMed: 19391135]

[49]. Albo D, Rothman VL, Roberts DD and Tuszynski GP 2000 Tumour cell thrombospondin-1 regulates tumour cell adhesion and invasion through the urokinase plasminogen activator receptor Br. J. Cancer 83 298–306 [PubMed: 10917542]

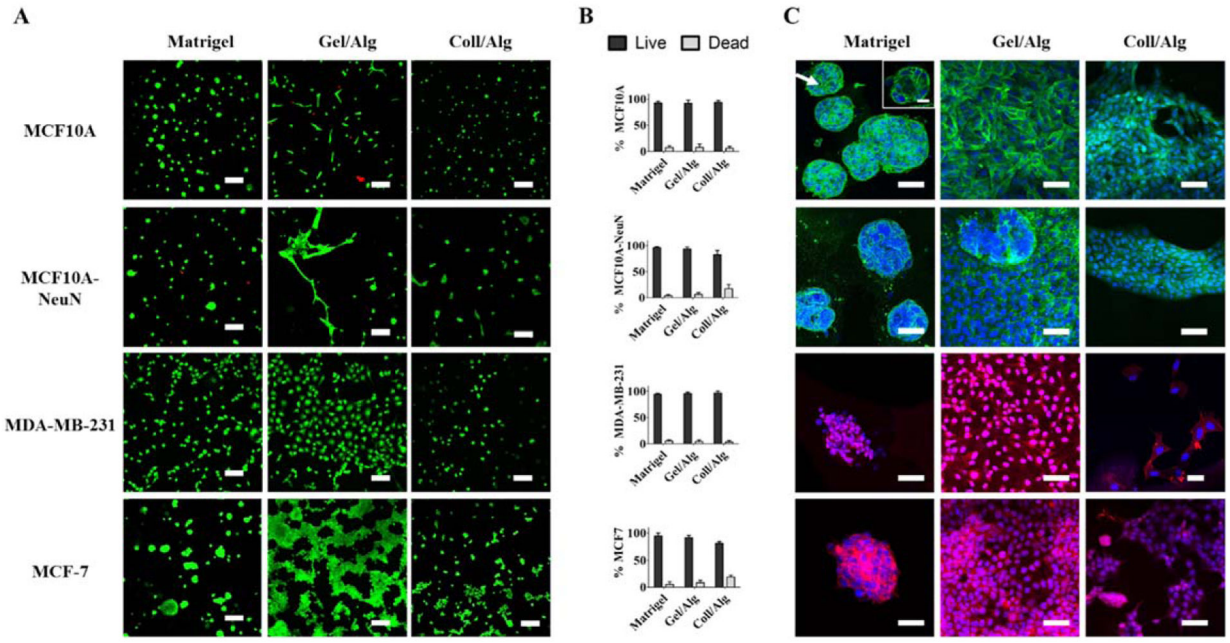

Figure 1.

Bioprinted breast epithelial cells only formed spheroids when printed in Matrigel bioink. Individual breast cells (MCF10A, MDA-MB-231, MCF10A-NeuN and MCF-7) were extrusion printed in three different bioinks (Matrigel, gelatin/alginate or collagen/alginate). (A) Representative Live/Dead images 24 h after printing (dead cells = red; live cells = green). Scale bar = 100 μm. (B) Quantification of live and dead cell percentages via ImageJ. (C) Representative confocal microscopy images of spheroid formation 5–8 d after bioprinting in Matrigel, gelatin/alginate or collagen/alginate (green = integrin α6, blue = Hoechst/nuclei and red = rhodamine phalloidin/actin). Scale bar = 50 μm; inset scale bar = 20 μm.

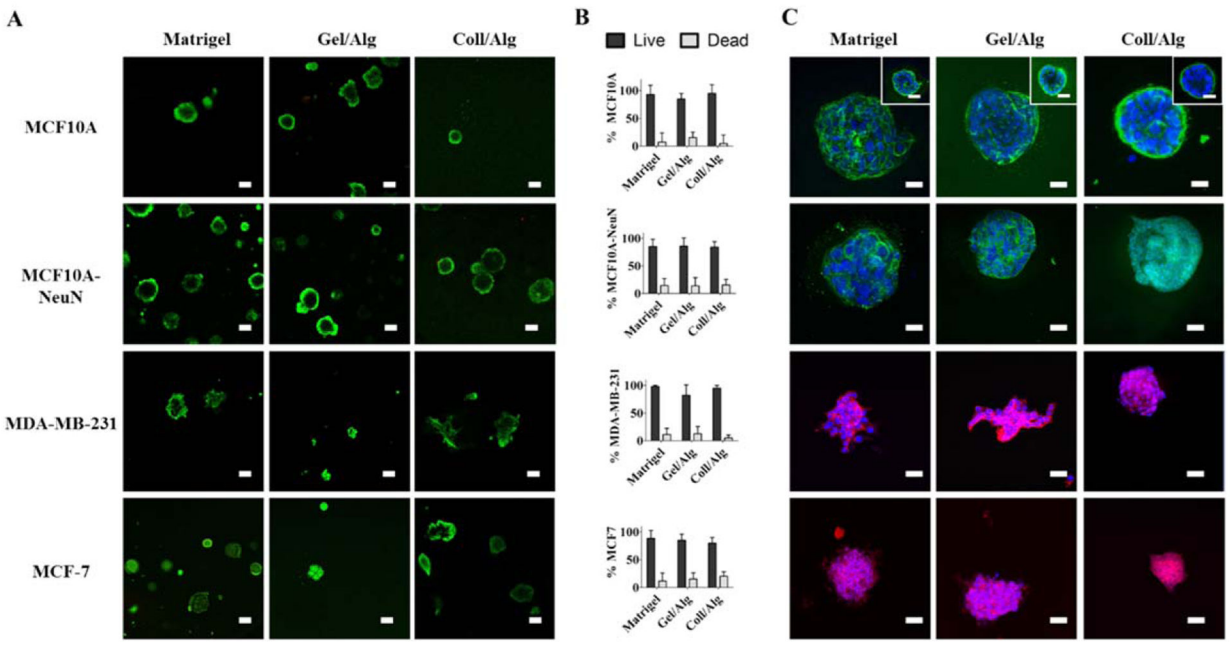

Figure 2.

Bioprinted 3D breast epithelial spheroids remained viable with typical spheroid morphology for 48 h. 3D breast spheroids (non-tumorigenic MCF10A and cancerous MDA-MB-231, MCF10A-NeuN and MCF-7) were extrusion bioprinted in Matrigel, gelatin/alginate or collagen/alginate. (A) Representative Live/Dead images 24 h after bioprinting (dead cells = red, live cells = green). Scale bar = 100 μm. (B) Quantification of live and dead cell percentages (ImageJ). (C) Representative confocal microscopy images of spheroids 48 h after bioprinting in Matrigel, gelatin/alginate or collagen/alginate (green = integrin α6, blue = Hoechst/nuclei, red = rhodamine phalloidin/actin). Scale bar = 50 μm; inset scale bar = 20 μm.

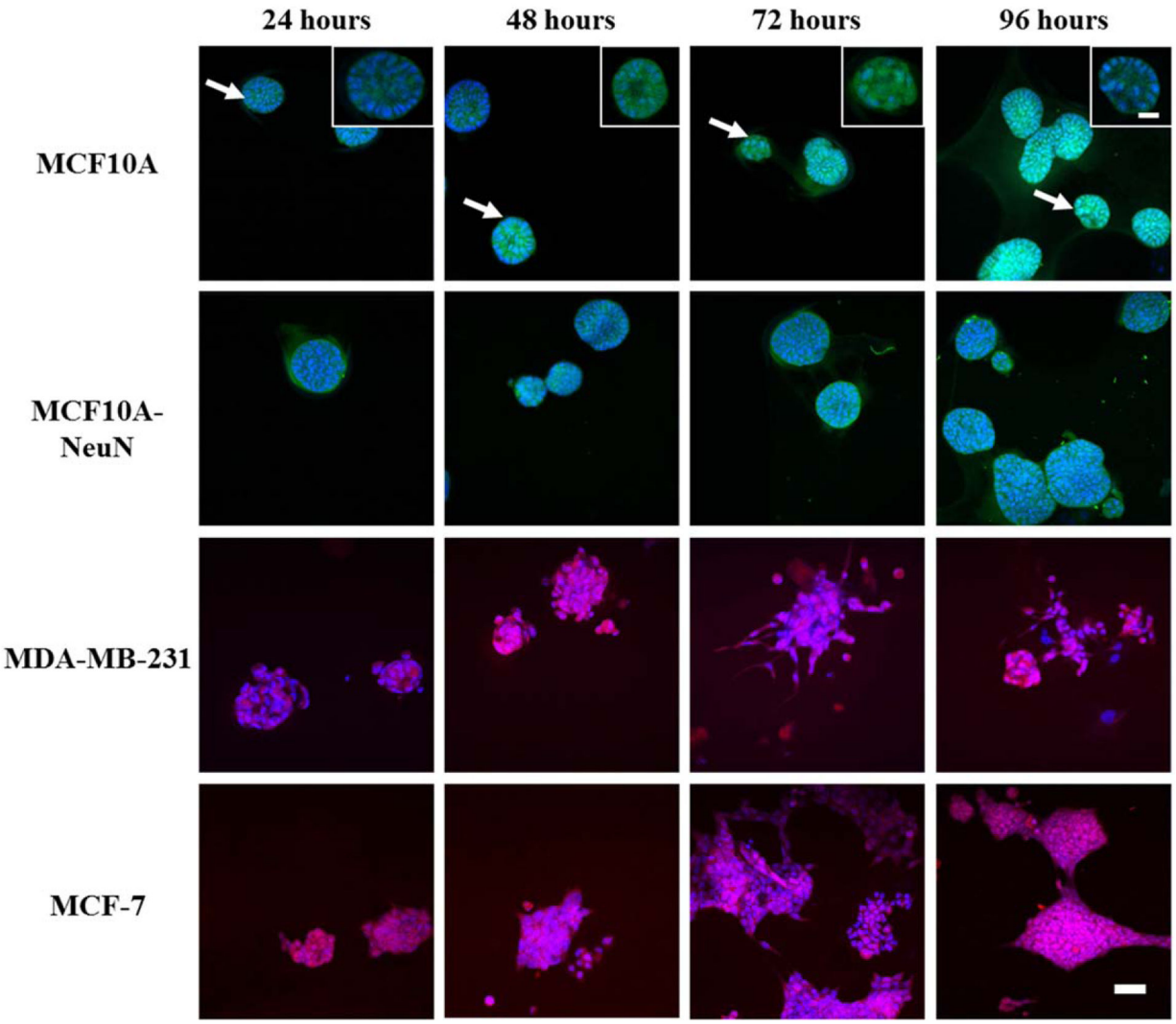

Figure 3.

Bioprinted 3D breast epithelial spheroids maintained typical spheroid morphology for 96 h in collagen/alginate bioink. 3D breast spheroids (non-tumorigenic MCF10A and cancerous MDA-MB-231, MCF10A-NeuN and MCF-7) were extrusion bioprinted in collagen/alginate bioink and then imaged by confocal microscopy (green = integrin α6, blue = Hoechst/nuclei, red = rhodamine phalloidin/actin). Scale bar = 50 μm; inset scale bar = 20 μm.

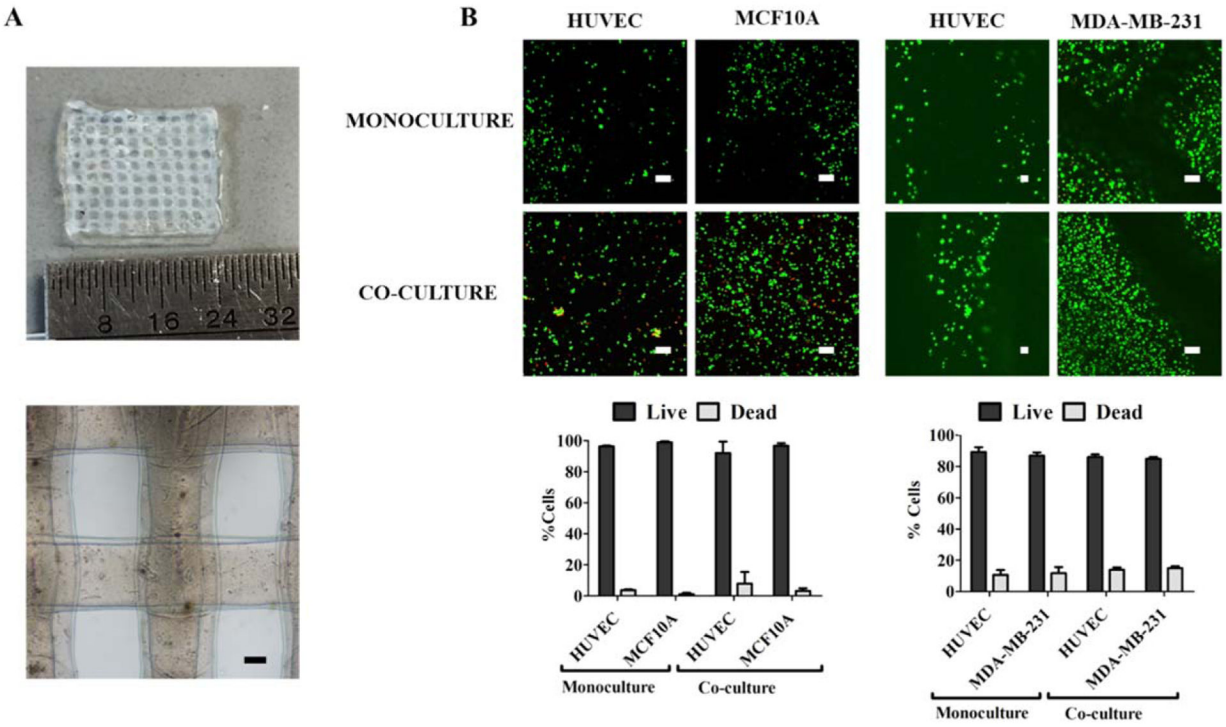

Figure 4.

Both mono- and co-cultures of vascular endothelial and individual breast epithelial cells remained viable after bioprinting in collagen-alginate bioink. Individual non-tumorigenic MCF10A or cancerous MDA-MB-231 spheroids were extrusion bioprinted in a grid with HUVEC collagen-alginate bioink. (A) Bioprinted grid structure used for co-culture experiments. Scale bar = 200 μm. (B) Confocal microscopy images of the Live/Dead assay (dead cells = red, live cells = green) and quantification of the live and dead cell percentages of both cells types in mono- and co-culture. Scale bar = 100 μm.

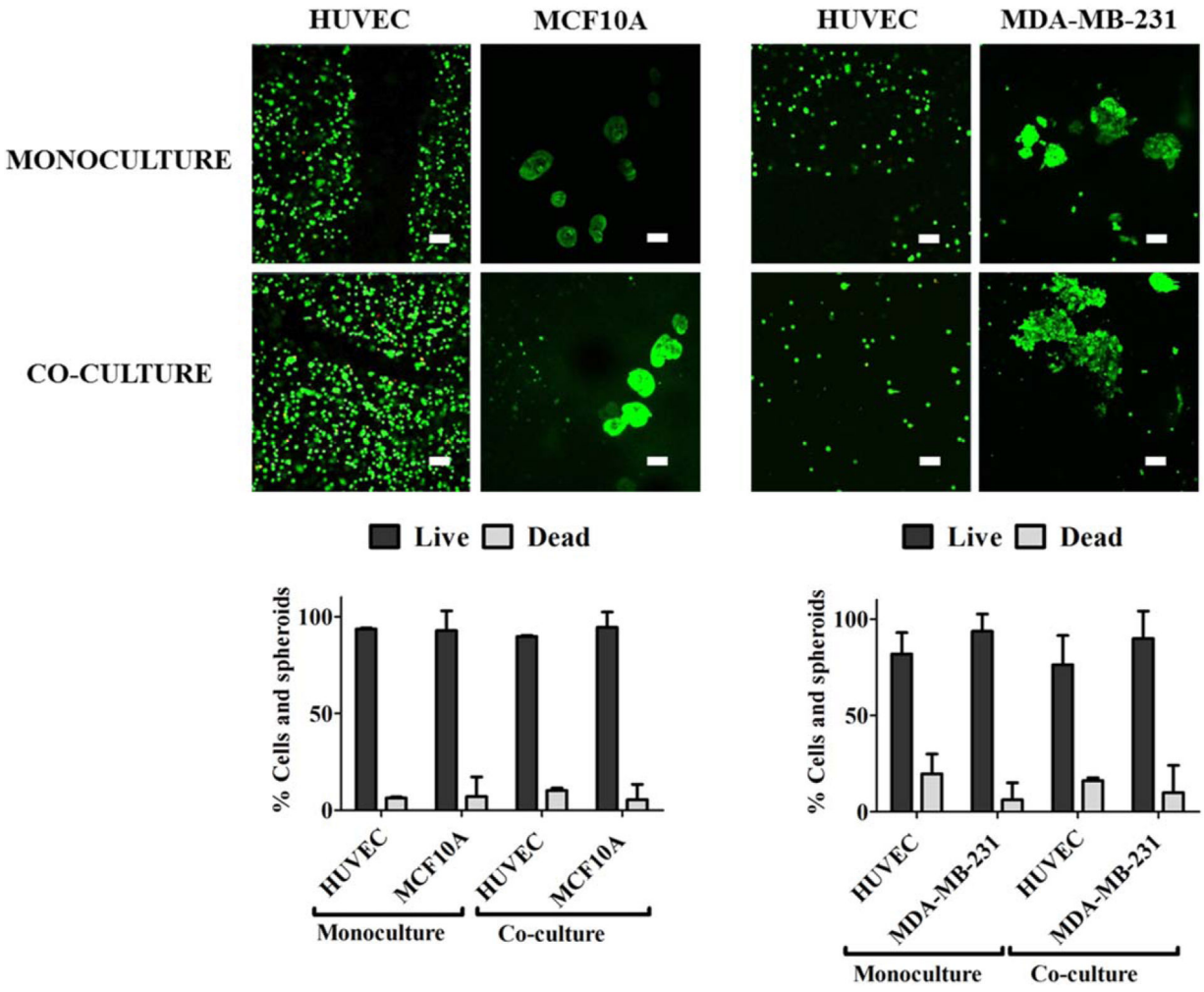

Figure 5.

3D breast epithelial spheroids remained viable when printed in a structure with endothelial cells. 3D non-tumorigenic MCF10A or cancerous MDA-MB-231 spheroids were extrusion bioprinted in a grid with HUVEC collagen-alginate bioink. Confocal microscopy images of the Live/Dead assay (dead cells = red, live cells = green) and quantification of the live and dead cell percentages of both cells types in mono- and co-culture. Scale bar = 100 μm.

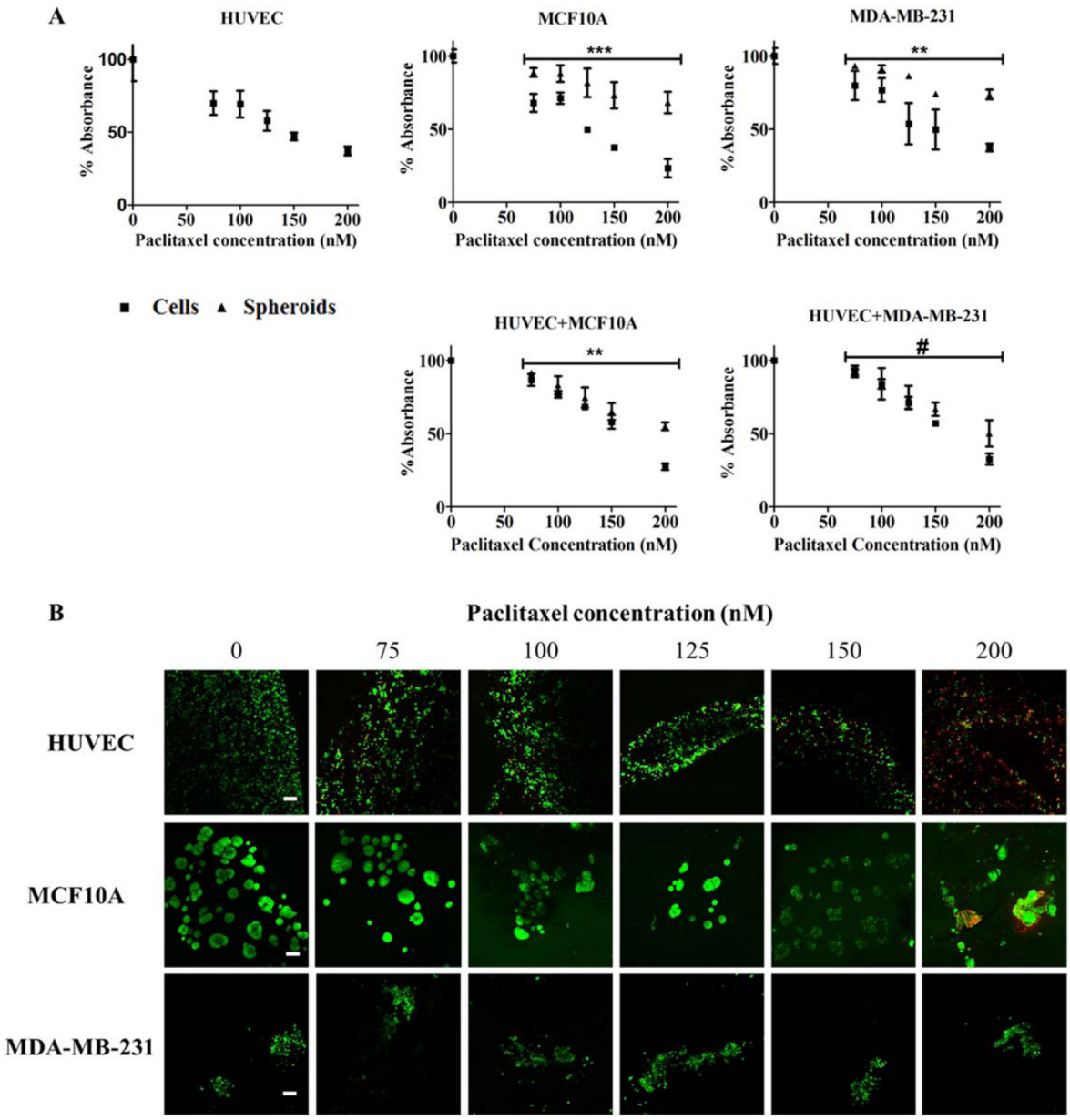

Figure 6.

Bioprinted 3D breast spheroids were more resistant to paclitaxel than individual cells, but this effect was abrogated in co-culture with endothelial cells. (A) Conditioned media from endothelial and breast epithelial mono- and co-cultures was incubated with resazurin 48 h after bioprinting, and relative absorbance was quantified in a microplate reader. # $p < 0.05$, ** $p < 0.001$, ***$p < 0.0001$ for spheroids as compared to cells by ANOVA. (B) Representative Live/Dead images (dead cells = red, live cells = green) from co-culture experiments showing HUVEC, MCF10A, or MDA-MB-231 bioprinted grid areas. Scale bar = 100 μm.